I&EC research
Industrial & Engineering Chemistry Research

Article

pubs.acs.org/IECR

Performance Simulation of Ionic Liquid and Hydrofluorocarbon Working Fluids for an Absorption Refrigeration System

Sarah Kim, Nishith Patel, and Paul A. Kohl*

School of Chemical and Biomolecular Engineering, Georgia Institute of Technology, Atlanta, Georgia 30332, United States

ABSTRACT: The theoretical performance of ionic-liquid- (IL-) based working fluids in an absorption refrigeration system was investigated. The IL 1-butyl-3-methylimidazolium hexafluorophosphate ([bmim][PF_6]) and five hydrofluorocarbons (HFCs) were selected as the absorbent and refrigerant, respectively. The Redlich−Kwong equation of state and two-phase pressure-drop model were used to compute the thermodynamic conditions and performance of the working-fluid pairs. The effects of the desorber and absorber temperatures, solution heat exchanger, and accessibility of waste heat on the system performance were evaluated. R152a showed the highest coefficient of performance, 57.3, when the desorber operated on waste heat only and the desorber and absorber were operated at 373.15 and 300.65 K, respectively. The friction-loss component of the total pumping work was below 2.5% of the pumping work for all refrigerants.

1. INTRODUCTION

The absorption refrigeration cycle based on an ionic-liquid (IL) working fluid is of interest as a means of utilizing low-quality waste heat. Absorption chillers offer an opportunity to recycle thermal energy; however, their use has been somewhat limited because of technological challenges, health hazards, and environmental concerns.[1] The commonly used absorption refrigeration working-fluid pairs ammonia/water and water/LiBr have drawbacks including toxicity (ammonia), negative effects of crystallization (LiBr), incompatibility with metal components, and the need for a rectifier for postdesorption separation of the fluid streams.[2] Further, the pressure and temperature of the evaporator in the ammonia/water and water/LiBr systems are significantly different from those of Freon-based vapor-compression systems, so that many refrigeration applications are not within reach.

ILs are liquid salts at ambient temperature and are being considered as absorbents in a variety of applications because of their tunable properties, zero vapor pressure, high thermal stability, and environmental safety.[3] In particular, the low volatility of ionic ILs enables easy separation of the volatile working fluid by thermal stratification. Several theoretical studies have evaluated the performance of IL-based working fluids including 1-ethyl-3-methylimidazolium ethylsulfate ([emim][EtSO4]);[4] 1,3-dimethylimidazolium dimethylphosphate ([emim][DMP]);[5] and various imidazolium-, pyridinium-, and pyrrolidinium-type ILs.[6,7] In a previous report, our group reported the first experimental demonstration of ionic liquid/Freon working fluids.[8]

The nonrandom two-liquid (NRTL) model has been commonly used to fit the experimental solubilities of refrigerants in absorbents because of its simplicity and good approximation of solubility values.[9,10] However, it is preferable to employ a model that can be used to calculate pure-component and mixture properties in multiphase systems in addition to having good accuracy over a wide range of temperatures and pressures. Theoretical solution models (including the NRTL model) are limited in their usefulness at temperatures below the refrigerant critical temperature, and the combined use of empirical fitting equations with the gas-phase equation of state (EOS) might not always be consistent at high generator temperatures.[12] In the case of pentafluoroethane (R125), the critical temperature is 351.56 K. Thus, the Redlich−Kwong-type EOS was employed here for improved modeling of the system. The EOS model allows computation of precise mixture properties, compositions, and state conditions such as mixture enthalpy, vapor quality, and fluid temperature. A two-phase pressure-drop equation was introduced into the EOS model to evaluate the friction losses due to pumping the viscous IL, which will affect the pumping work and system efficiency. In this study, 1-butyl-3-methylimidazolium hexafluorophosphate ([bmim][PF_6]) was used as the IL, and five different hydrofluorocarbon (HFC) refrigerants (R134a, R32, R125, R143a, R152a) were analyzed. The effects of a counterflowing solution heat exchanger, desorber temperature, and absorber temperature on the system performance were investigated.

2. SYSTEM ANALYSIS

2.1. Thermodynamic Model. The principal features of the absorption refrigeration cycle are shown in Figure 1. The cycle resembles that of the vapor-compression refrigeration (heat-pump) system, except the vapor compressor is replaced with a thermochemical process consisting of an absorber, a liquid pump, a solution heat exchanger, a desorber, and an expansion device. Pressurization of the thermochemical process starts in the absorber, where the refrigerant vapor from the evaporator (state point 2) is exothermically absorbed into the strong-IL solution (state point 10), resulting in a weak-IL solution at state point 5. The IL solution is pressurized by the liquid pump after the absorber. Then, the solution (regenerative) heat exchanger preheats the weak-IL solution at state point 6, creating state

Received: January 23, 2013
Revised: April 11, 2013
Accepted: April 19, 2013
Published: April 19, 2013

   dx.doi.org/10.1021/ie400261g | *Ind. Eng. Chem. Res.* 2013, 52, 6329−6335

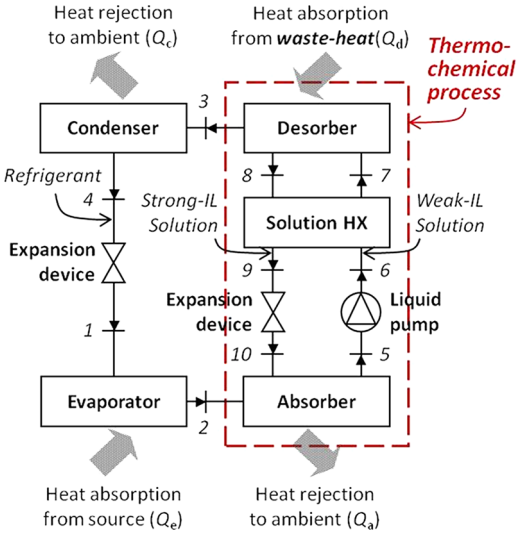

Figure 1. Schematic diagram of an absorption refrigeration system using an IL/refrigerant mixture as the working fluid.

point 7 using heat from the strong-IL solution flowing back to the absorber (from the desorber). In the desorber, superheated refrigerant vapor is released at high temperature and pressure from the IL through desorption from the weak-IL solution by the addition of heat (preferably waste heat). The strong IL returns to the absorber through the solution heat exchanger and an expansion device. The condensation/absorption process at the absorber and the vaporization/desorption process at the desorber both occur in the liquid phase. This allows use of a liquid pump to create the pressure difference between the condenser and the evaporator.

In this work, system-level simulations were carried out with refrigerant/ionic liquid combinations. In all calculations, the operating temperatures of the condenser and evaporator were set to 50 and 25 °C, respectively. The cooling capacity at the evaporator was set to 100 W. The energy and mass conservation equations for all components in the system were simultaneously solved to determine the heat and workloads. The overall energy balance for the system is given by

$$Q_d + Q_e + W_p = Q_c + Q_a \tag{1}$$

where W_p is the liquid pump work and Q is the heat input/output. The subscripts d, e, c, and a correspond to the desorber, evaporator, condenser, and absorber, respectively. All values of heat are expressed as positive (magnitude) values regardless of the direction (in or out) of heat flow.

A counterflow-type heat exchanger was used to recover heat from the strong-IL solution and to reduce the heat supply to the desorber (Q_d). One stream in the counterflow heat exchanger can undergo a greater temperature change than the other because of the unequal heat-capacity values and mass flow rates for the weak and strong streams. The heat-capacity rate is defined by the equation

$$C = mC_p \tag{2}$$

where C is the heat-capacity rate, m is the mass flow rate, and C_p is the heat capacity. The heat-capacity coefficients, C_{hot} and C_{cold}, can be calculated for both inlet streams by the equations

$$C_{hot} = m_{hot}C_{p,hot} \tag{3}$$

$$C_{cold} = m_{cold}C_{p,cold} \tag{4}$$

Together, eqs 2−4 and can be used to determine which stream will limit the amount of heat transfer.[13] Specifically, the heat transfer is limited by the minimum value of the two heat-capacity coefficients

$$C_{min} = \begin{cases} C_{hot}, & C_{hot} \le C_{cold} \\ C_{cold}, & C_{cold} < C_{hot} \end{cases} \tag{5}$$

The maximum possible heat transfer for an adiabatic, infinitely long counterflow heat exchanger is given by

$$Q_{max} = C_{min}(T_{hot,in} - T_{cold,in}) \tag{6}$$

However, a real heat exchanger can achieve only a fraction of the maximum possible heat transfer depending on its efficiency, φ

$$Q_{actual} = \varphi Q_{max}, \quad 0 \le \varphi \le 1 \tag{7}$$

For the calculations, two values of heat exchanger efficiency, 25% and 40% (i.e., φ = 0.25 or 0.40), were used and compared. The estimated heat transfer for φ = 0.25 is thus given by

$$Q_{actual} = 0.25Q_{max} = 0.25C_{min}(T_{hot,in} - T_{cold,in}) \tag{8}$$

This estimate of the heat transfer at the counterflow heat exchanger can then be used to determine the temperature and enthalpy of the exit streams of the solution heat exchanger.

The energy conservation for a subsystem consisting of a regenerative heat exchanger and a pump is given by

$$(h_9 - h_8)(m_w - m_r) = (h_7 - h_5)m_w - W_p \tag{9}$$

In eq 9, h is the enthalpy, and the subscripts correspond to the locations shown in the system diagram, Figure 1. Also, m_w and m_r are the mass flow rates of the weak-IL solution and the refrigerant leaving the desorber, respectively. Energy conservation for the desorber is given by

$$Q_d = h_8(m_w - m_r) + h_3m_r - h_7m_w \tag{10}$$

Similarly, the heat rejected at the absorber is given by

$$Q_a = h_5m_w - h_{10}(m_w - m_r) - h_2m_r \tag{11}$$

Energy conservation for the condenser and evaporator yields the corresponding heat loads

$$Q_c = (h_4 - h_3)m_r \tag{12}$$

$$Q_e = (h_2 - h_1)m_r \tag{13}$$

The cooling-to-total-energy (CE) ratio is defined as the heat removed at the evaporator divided by the power supplied to the desorber and the pump

$$CE = Q_e/(Q_d + W_p) \tag{14}$$

Because waste heat is intended to be used to heat the desorber, the practical coefficient of performance, η, is defined by

$$\eta = \frac{Q_e}{W_p} \tag{15}$$

Equation 15 is the usual figure of merit for absorption refrigeration/heat pump systems where waste heat is used.

In this analysis, the Redlich−Kwong (RK) EOS was used to calculate the thermodynamic properties of the fluids at each

dx.doi.org/10.1021/ie400261g | Ind. Eng. Chem. Res. 2013, 52, 6329−6335

Table 1. Critical Properties and EOS Constants of [bmim][PF_6] and HFC Refrigerants

pure compound	T_c (K)	P_c (kPa)	β_0	β_1	β_2	β_3
[bmim][PF_6][16]	860.5	2645	1.0	0.62627	0	0
R32[12]	351.26	5782	1.0019	0.48333	−0.07538	0.00673
R125[12]	339.19	3637	1.0001	0.47736	−0.01977	−0.0177
R134a[12]	374.21	4059	1.0025	0.50532	−0.04983	0
R143a[12]	346.20	3759	1.0006	0.45874	−0.04846	−0.0143
R152a[12]	386.44	4520	1.0012	0.48495	−0.08508	0.0146

point in the cycle. Binary interaction parameters were introduced to improve the accuracy of the model. Several assumptions were made for convenience in the calculations: (i) the expansion process is isenthalpic, (ii) the compression process is isentropic, (iii) state 4 is saturated liquid refrigerant, (iv) state 2 is saturated vapor refrigerant, and (v) the vapor quality at state 5 is zero.

The general RK EOS can be written in the form[11]

$$P = \frac{RT}{V-b} - \frac{a(T)}{V(V+b)} \tag{16}$$

with

$$a(T) = 0.42748\frac{R^2T_c^{\,2}}{P_c}\alpha(T) \tag{17}$$

and

$$b = 0.08664\frac{RT_c}{P_c} \tag{18}$$

In eqs 16−18, P is the pressure, T is the temperature, V is the molar volume, R is the gas constant, a and b are constants, and the subscript c represents the critical properties of the substance. The temperature-dependent function of the parameter α is expressed as

$$\alpha(T) = \sum_{k=0}^{\leq 3}\beta_k\left(\frac{1}{T_r} - T_r\right)^k, \quad T_r \equiv T/T_c \tag{19}$$

The parameter β_k was determined so as to yield the vapor pressure of each pure compound, the refrigerant and the ionic liquid.[12] The vapor pressure of the ionic liquid is practically zero, and data for the critical parameters (T_c and P_c) are not available. A rough estimate of critical constants based on liquid densities alone is generally sufficient for correlating the solubility data of high-boiling-point compounds at operating conditions.[14] However, the temperature-dependent part of the absorbent is important for refrigerant/absorbent mixtures, and therefore, β for the absorbent was modeled by two terms that were treated as adjustable fitting parameters. The critical properties along with the β values are summarized in Table 1.

Three binary interaction parameters (BIPs), τ, l, and k, were introduced for the a and b parameters for N-component mixtures[15]

$$a = \sum_{i,j=1}^{N}\sqrt{a_i a_j}f_{ij}(T)(1-l_{ij})x_i x_j, \qquad a_i = 0.42748\frac{R^2T_{ci}^{\,2}}{P_{ci}}\alpha(T) \tag{20}$$

$$f_{ij}(T) = 1 + \tau_{ij}/T, \qquad \text{where } \tau_{ij} = \tau_{ji} \text{ and } \tau_{ii} = 0 \tag{21}$$

$$b = \frac{1}{2}\sum_{i,j=1}^{N}(b_i + b_j)(1-l_{ij})(1-k_{ij})x_i x_j,$$

$$b_i = 0.08664\frac{RT_{ci}}{P_{ci}} \tag{22}$$

Also, the following relationships hold: $l_{ij} = l_{ji}$, $l_{ii} = 0$, $k_{ij} = k_{ji}$, $k_{ii} = 0$.

Phase equilibria for an N-component system can be obtained by solving equilibrium conditions, eq 23,

$$x_i^{\alpha}\phi_i^{\alpha} = x_i^{\beta}\phi_i^{\beta} = x_i^{\gamma}\phi_i^{\gamma} = \cdots, \qquad i = 1, \ldots, N \tag{23}$$

where x_i^{α}, x_i^{β}, x_i^{γ}, ..., are the mole fractions of the ith species in the α, β, γ, ..., coexisting phases and ϕ_i^{α}, ϕ_i^{β}, ϕ_i^{γ}, ..., are the fugacity coefficients of the ith species in the corresponding phases. The fugacity coefficients can be calculated from the equations[15]

$$\ln\phi_i = \int_V^{\infty}\left\{\left(\frac{\partial(nZ)}{\partial n_i}\right)_{T,nV,n_j} - 1\right\}\frac{dV}{V} - \ln Z \tag{24}$$

$$Z = \frac{PV}{RT} \tag{25}$$

The equilibrium condition (eq 23) is used to compute the solubility of a refrigerant in the IL at a given temperature and pressure. The optimum BIPs were found in a previous study and are listed in Table 2.

Table 2. Binary Interaction Parameters for [bmim][PF_6] and HFC Refrigerants[8]

fluid pair	$l_{12} = l_{21}$	k_{12}	τ_{12} (K)	ΔP^a (MPa)
R32/[bmim][PF_6]	0.0295	−0.0167	13.9407	0.010
R125/[bmim][PF_6]	0.1865	−0.2545	78.5937	0.009
R134a/[bmim][PF_6]	0.1278	−0.1504	41.9269	0.005
R143a/[bmim][PF_6]	−0.239	0.1948	50.1348	0.004
R152a/[bmim][PF_6]	−0.2496	0.2112	70.1631	0.006

[a]Standard deviations of nonlinear least-squares fits in pressures.

The EOS was then used to find the enthalpy values at the point of interest, according to the equation

$$H = H^R + \int_{T_0}^{T}\sum_{i=1}^{N}x_i C_{pi}^0\,dT + H_0 \tag{26}$$

where H^R is the residual enthalpy; T_0 is the reference temperature, which was set to 273.15 K; and H_0 is an arbitrary constant (an enthalpy at the reference state). The ideal-gas heat capacity of the ith species, C_{pi}^0, was modeled as

$$C_{pi}^0 = C_0 + C_1T + C_2T^2 + C_3T^3 \tag{27}$$

dx.doi.org/10.1021/ie400261g | Ind. Eng. Chem. Res. 2013, 52, 6329−6335

Table 3. Coefficients for Ideal-Gas Heat Capacities of Pure Compounds (J·mol^{-1})

pure compound	C_0 (J·mol^{-1})	C_1 (J·mol^{-1}·K^{-1})	C_2 (J·mol^{-1}·K^{-2})	C_3 (J·mol^{-1}·K^{-3})
[bmim][PF$_6$][3]	−2.214	0.57685	-3.854×10^{-4}	9.785×10^{-8}
R32[12]	20.34	0.07534	1.872×10^{-5}	-3.116×10^{-8}
R125[12]	16.58	0.33983	-2.873×10^{-4}	8.870×10^{-8}
R134a[12]	12.89	0.30500	-2.342×10^{-4}	6.852×10^{-8}
R143a[12]	5.740	0.31388	-2.595×10^{-4}	8.410×10^{-8}
R152a[12]	8.670	0.2394	-1.456×10^{-4}	3.392×10^{-8}

The coefficients in eq 27 are listed in Table 3. Using the heat capacity for each species in the mixture, the enthalpy for the RK EOS is given by

$$H = \left(\frac{a}{b} - \frac{T}{b}\frac{da}{dT}\right)\ln\frac{V}{V+b} + RT(Z-1) + \int_{T_0}^{T}\sum_{i=1}^{N} x_i C_{pi}^{0}\, dT + H_0 \quad (28)$$

2.2. Pressure Drop. The viscosities of ILs are often relatively high. For example, [bmim][PF$_6$] at 294 K and atmospheric pressure has a viscosity of 376 mPa·s.[17] Thus, the IL flow in the microchannels used at the absorber and desorber could create a significant pressure drop, which could affect the system performance. The average pressure drop through the microfluidic channel heat exchangers was evaluated using the two-phase pressure-drop equation[18]

$$-\left(\frac{dP}{dz}\right) = \left[\frac{2f_l G_m{}^2(1-x^v)}{d_h\rho_l}\right]\varphi_l{}^2 + G_m{}^2\frac{d}{dz}\left[\frac{(x^v)^2}{\varepsilon\rho_v} + \frac{(1-x^v)^2}{(1-\varepsilon)\rho_l}\right] \quad (29)$$

In eq 29, d_h is the hydraulic diameter of the channel; and f, G, x^v, ρ, and ε are the liquid-phase fanning friction factor, mass flux, vapor quality, density, and void fraction, respectively. z is the axial direction coordinate along the channel length. The subscripts l and v stand for the liquid and vapor phases, respectively. In the two-phase multiplier correlation of Lockhart and Martinelli,[19] φ_l was incorporated with the C value proposed by Lee and Mudawar,[20] as follows

$$\varphi_l{}^2 = 1 + \frac{C}{X} + \frac{1}{X^2} \quad (30)$$

$$C = 2.16 Re_{lo}{}^{0.047} We_{lo}{}^{0.6} \quad \text{(laminar liquid−laminar vapor)} \quad (31)$$

$$C = 1.45 Re_{lo}{}^{0.25} We_{lo}{}^{0.23} \quad \text{(laminar liquid−turbulent vapor)} \quad (32)$$

where Re_{lo} and We_{lo} are the liquid-only Reynolds and Weber numbers, respectively. The Martinelli parameter, X, and the single-phase empirical correlation of the fanning friction factor for laminar flow in a rectangular channel by Shah and London[21] are expressed as

$$X = \left(\frac{\mu_l}{\mu_v}\right)^{0.5}\left(\frac{1-x^v}{x^v}\right)^{0.5}\left(\frac{\rho_v}{\rho_l}\right)^{0.5} \quad (33)$$

$$f \times Re = 24(1 - 1.3553\beta + 1.9467\beta^2 - 1.7012\beta^3 + 0.9564\beta^4 - 0.2537\beta^5) \quad (34)$$

In eq 33, μ is the viscosity, and β is the aspect ratio of the channel. Also, the void-fraction model of Zivi[22] was employed in this study. Microchannel structures were used in the absorber and desorber in this study because of their high heat- and mass-transfer rates. However, the magnitude of the negative effects of the high IL viscosity on the pressure drop within the microchannel heat exchangers and, in turn, the system performance was critically assessed in this study. The dimensions (length × width) of the evaporator and condenser were 2 × 2 cm and 3 × 3 cm, respectively. The dimensions of the absorber and the desorber were 8 × 8 cm. The microfluidic channel cross-sectional area for the heat exchangers was 1 × 1 mm.

3. RESULTS AND DISCUSSION

The fluorocarbon/IL absorption refrigeration cycle was previously demonstrated, and a limited number of system parameters were investigated.[7,8] In this study, the EOS model described in the preceding section was used to investigate the performance of five fluorocarbons as refrigerants and the specific absorber and desorber performance operating parameters.

3.1. Effects of Absorber/Desorber Outlet Temperature on CE Ratio and η. It was previously shown that CE ratio has a parabolic shape with respect to desorber outlet temperature.[8] In this study, the CE ratios for five different fluorocarbon refrigerants were compared (Figure 2). Although

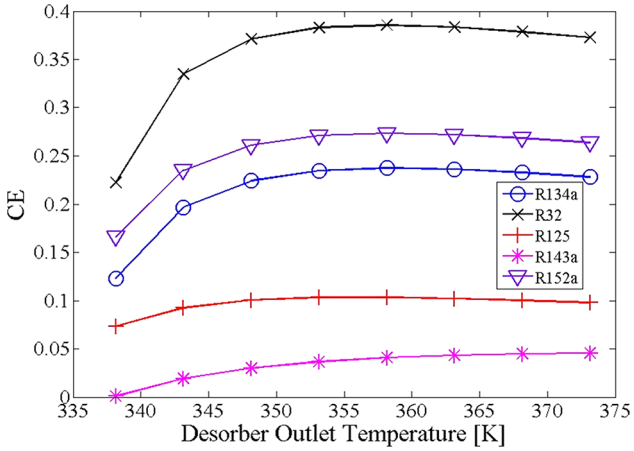

Figure 2. Effects of desorber outlet temperature on CE ratio (without solution heat exchanger). T_a = 309.65 K.

the five refrigerants in Figure 2 are all low-molecular-weight fluorocarbons, there is a significant difference among the CE values, regardless of desorber temperature. Four of the five refrigerants consist of fluorinated ethane with two (R152a), three (R143a), four (R134a), or five (R125) fluorine atoms. R32 (difluoromethane) and R143a had the highest and lowest

dx.doi.org/10.1021/ie400261g | Ind. Eng. Chem. Res. 2013, 52, 6329−6335

CE values, respectively. Within the set of fluoroethanes, there was no trend with the degree of fluorination. However, the trend in efficiency did follow the solubility of the refrigerants in [bmim][PF_6], which emphasizes the importance of refrigerant solubility in the absorbent.[8] The main difference between the refrigerants was the low solubility of the refrigerant in the IL at the absorber temperature and pressure. A low solubility of the refrigerant in the IL at the absorber leads to a small solubility difference between the absorber and desorber. When the solubility difference between absorber and desorber is small, larger quantities of IL have to be recirculated in the thermochemical compressor to achieve the same refrigerant flow. On each pass of the IL through the thermochemical compressor, the IL has to be heated to the desorber temperature and then cooled to the absorber temperature, which consumes energy at the desorber.

At the lower temperature values in Figure 2, the fluorocarbon solubility difference between the desorber and absorber became small and resulted in a lower net refrigerant flow per unit flow of the IL. The CE ratio decreased because less refrigerant was released at the desorber for each pass of the IL from the absorber to the desorber. Each pass of the IL required energy (i.e., waste heat) to heat the IL at the desorber to the highest temperature. Heat was then discharged at the absorber to decrease the temperature so that the refrigerant could be absorbed there. This heating and cooling of the IL on each pass of the IL did not directly produce refrigerant vapor at the condenser; it simply brought the IL to the highest and lowest temperatures for desorption and absorption, respectively.

At higher temperatures, the solubilities of the refrigerants in the IL at the desorber were already very low. Raising the temperature of the IL to even higher values resulted in only a small increase in the flow rate of the refrigerant at the exit of the desorber. The result was that additional waste heat had to be used to raise the IL temperature at the desorber, with little gain in cooling capacity.

The effect of decreasing the absorber temperature from 309.65 K (Figure 2) to 300.65 K is shown in Figure 3 for the five fluorocarbons. When the absorber temperature was decreased nearly to that of the evaporator, 298.15 K, the solubility difference between the absorber and desorber became significant even at relatively low desorber temperatures. This removed the exponential behavior at the lower temperature limit in Figure 2 and resulted in a reverse relationship between the CE ratio and the desorber outlet temperature. Decreasing the absorber temperature to 300.65 from 309.65 K resulted in an increase in the CE ratio for each of the five refrigerants. The CE ratio improved by a maximum factor of 4.2, 2.9, 3.1, 60.9, and 3.2 for refrigerants R134a, R32, R125, R143a, and R152a, respectively. This maximum effect was observed at a desorber temperature of 338.15 K.

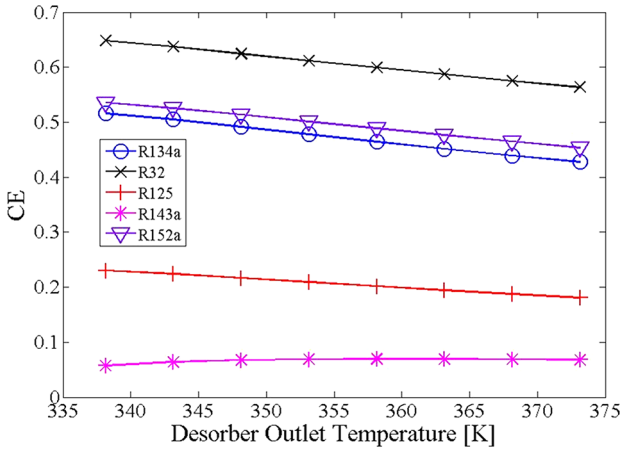

Figure 3. Effects of desorber outlet temperature on CE ratio (without solution heat exchanger). T_a = 300.65 K.

The effect of desorber temperature on η was investigated for each refrigerant, as shown in Figure 4 for an absorber temperature of 309.65 K. The coefficient of performance, η, considers only the energy to pump the IL in the thermochemical compressor and uses waste heat to drive the desorber. η increased continuously with increasing desorber outlet temperature. This is because the net refrigerant flow passing through the evaporator per unit IL flow rate is the most important factor. Increasing the net refrigerant flow rate per unit IL flow rate reduces the pumping work. When only low-grade waste heat (~70 °C) is available at the desorber, the absorber temperature becomes an important factor in achieving higher η values because of the small solubility difference between the absorber and desorber. The maximum impact of desorber temperature was observed at 338.15 K.

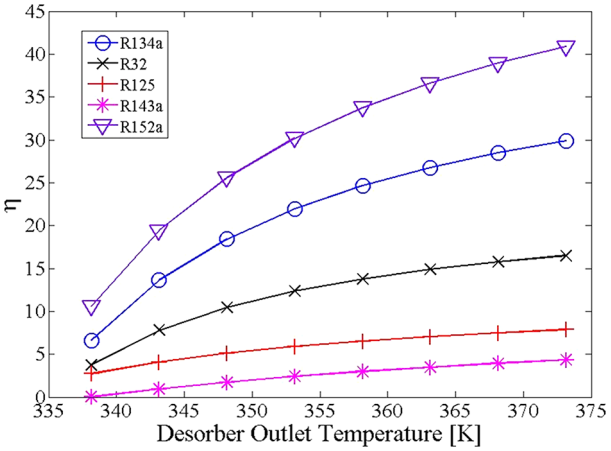

Figure 4. Effects of desorber outlet temperature on η (without solution heat exchanger). T_a = 309.65 K.

Decreasing the absorber temperature from 309.65 to 300.65 K resulted in a higher coefficient of performance (Figure 5). Similarly to the CE ratio, η was less sensitive to desorber temperature at lower absorber temperatures because there was a larger solubility difference between the absorber and desorber when the absorber was at 300.65 K. The values of η in Figure 5 (absorber at 300.65 K) are larger than the values of η in Figure 4 (absorber at 309.65 K) by factors of 5.17, 3.78, 3.98, 81.3, and 4.4 for R134a, R32, R125, R143a, and R152a, respectively. The improvement factor was most dramatic for refrigerants that have relatively low solubilities at the absorber, such as R143a in [bmim][PF_6].

3.2. Effects of Solution Heat Exchanger on CE Ratio.

The solution heat exchanger transfers heat from the strong-IL solution at system point 8 to the weak-IL solution at system point 6 (Figure 1). The heat exchanger improves the system efficiency because it reduces the waste heat needed to increase the temperature of the IL in the desorber and reduces the amount of heat discharged at the absorber. Aphornratana and Sriveerakul reported that an experimental 2-kW cooling-

dx.doi.org/10.1021/ie400261g | Ind. Eng. Chem. Res. 2013, 52, 6329−6335

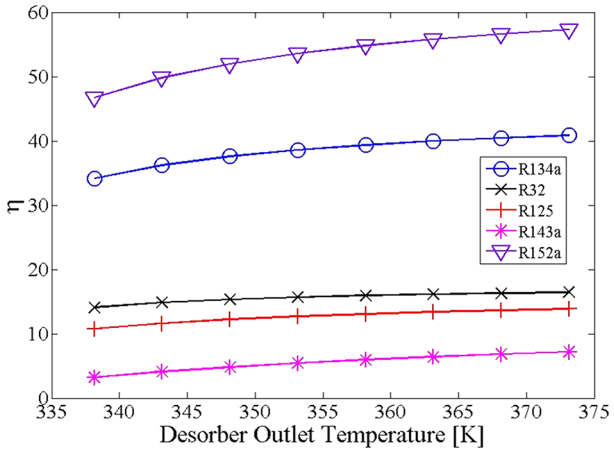

Figure 5. Effects of desorber outlet temperature on η (without solution heat exchanger). T_a = 300.65 K.

capacity refrigerator showed a 60% increase in CE ratio when three double-pipe solution heat exchangers were introduced.[23] The CE ratio was calculated for a system with a 25% efficiency solution heat exchanger, as shown in Figure 6. The weak

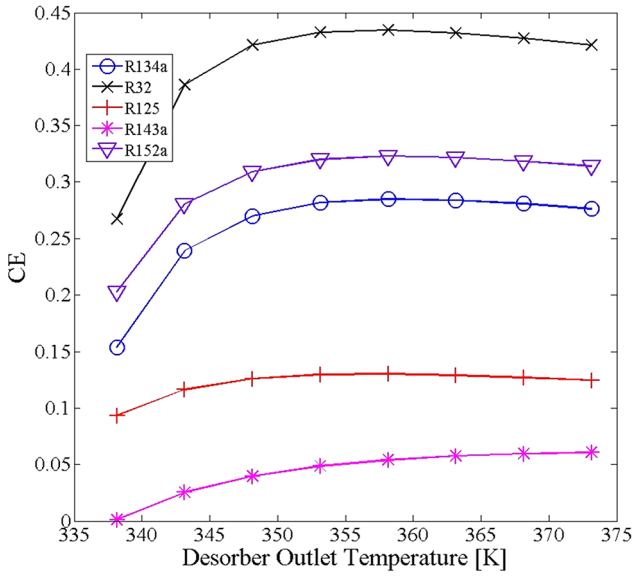

Figure 6. Effects of desorber outlet temperature on CE ratio (with solution heat exchanger). T_a = 309.65 K.

desorber inlet solution was preheated at the adiabatic solution heat exchanger using the higher-temperature strong solution leaving the desorber. Twenty-five percent of the available heat was exchanged. A comparison of Figure 2 (CE ratio without heat exchanger) and Figure 6 (CE ratio with heat exchanger) shows that the CE ratio increased by as much as 25%, 20%, 27%, 33%, and 22% for R134a, R32, R125, R143a, and R152a, respectively. The CE ratio increased by a greater factor when a more efficient heat exchanger, 40% efficiency, was used. The improvements in CE ratio were up to 47%, 37%, 52%, 66%, and 41% for R134a, R32, R125, R143a, and R152a, respectively, when the 40% efficient heat exchanger was used.

3.3. Effects of Friction Loss. A potential drawback using an IL in an absorption refrigeration cycle is the friction loss during pumping of the relatively high-viscosity IL fluid. The friction loss for each of the five refrigerants decreased exponentially with respect to desorber temperature, as shown in Figure 7. Mixtures with higher refrigerant absorbances resulted in lower friction losses, because less IL was required to deliver the same amount of cooling.

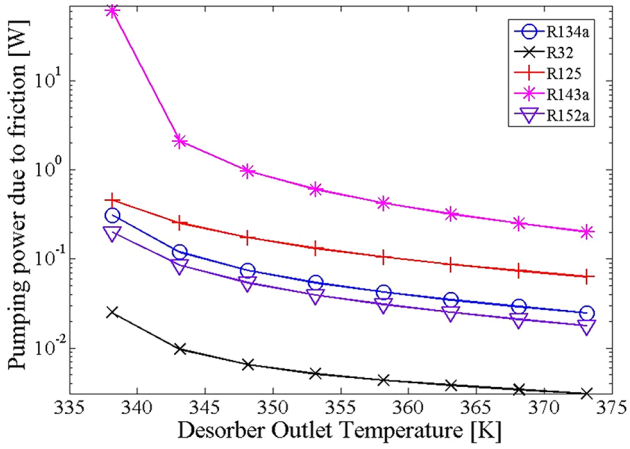

Figure 7. Pumping power due to friction (without solution heat exchanger), T_a = 309.65 K.

Refrigerants that had relatively low solubilities in [bmim][PF_6] (e.g., R143a and R125) had relatively large friction losses, especially at low desorber temperatures. However, even though some refrigerants had low solubilities in the IL, resulting in higher pumping losses, the overall contribution of the friction losses to the total pumping work was small for all five refrigerants. The total pumping work of the system was calculated by the equation

$$W_p = \dot{m}_s(P_c - P_e + \Delta P_{friction}) \quad (35)$$

Even in the case of R143a, the pumping work due to friction loss was less than 2.5% of the total pumping work, as shown in Figure 8. Thus, the effect of IL viscosity was found to be insignificant with respect to the IL pumping work.

4. CONCLUSIONS

The IL [bmim][PF_6] and five HFC refrigerants were investigated as working-fluid pairs for an absorption refrigeration system. The theoretical performance was evaluated using

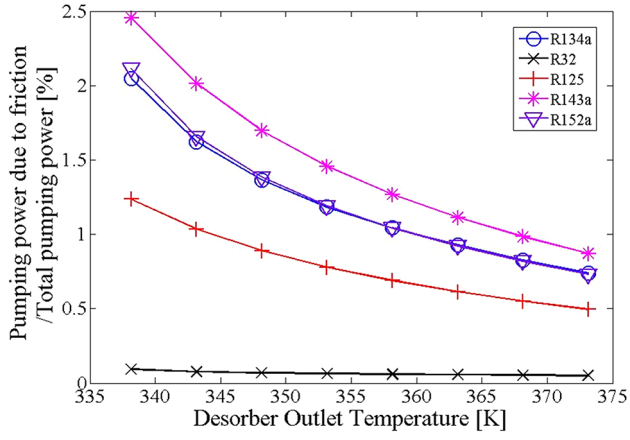

Figure 8. Required pumping work due to friction loss (without solution heat exchanger), T_a = 309.65 K.

dx.doi.org/10.1021/ie400261g | Ind. Eng. Chem. Res. 2013, 52, 6329−6335

the Redlich−Kwong EOS and two-phase pressure-drop calculations. Both the CE ratio and the coefficient of performance, η, had higher values at lower absorber temperatures. However, the response of the CE ratio had a maximum value with respect to desorber temperature, depending on the absorber temperature. The trends between solubility and performance found in this work provide useful guidance in the operation and efficiency of IL-based absorption refrigeration systems for cases in which limited waste heat (CE ratio) or excess waste heat (η) are available. The working-fluid pairs showed excellent coefficients of performance, η, when waste heat was used to drive the desorber. The introduction of a solution heat exchanger improved the system performance by decreasing the amount of heat required at the desorber and minimizing the heat discharged at the absorber. The effects of pumping losses due to friction during pumping of the IL were small and insignificant with respect to the total pumping energy.

AUTHOR INFORMATION

Corresponding Author

*E-mail: kohl@gatech.edu.

Notes

The authors declare no competing financial interest.

ACKNOWLEDGMENTS

The financial support of the Interconnect Focus Center, one of six focus centers of the Semiconductor Research Corporation, is gratefully acknowledged.

REFERENCES

(1) Sen, M.; Paolucci, S. Using Carbon Dioxide and Ionic Liquids for Absorption Refrigeration. In *7th IIR Gustav Lorentzen Conference on Natural Working Fluids*; International Institute of Refrigeration: Paris, 2006; pp 160−163.

(2) Srikhirin, P.; Aphornratana, S.; Chungpaibulpatana, S. A review of absorption refrigeration technologies. *Renewable Sustainable Energy Rev.* **2001**, *5* (4), 343−372.

(3) Shiflett, M. B.; Yokozeki, A. *Absorption cycle utilizing ionic liquid as working fluid*. U.S. Patent 2006-0197053 A1, 2006.

(4) Sen, M.; Paolucci, S.; Liu, W. Analysis of the performance of ionic liquids in cooling loops. In *ASME International Mechanical Engineering Congress and Exposition, IMECE 2007*; American Society of Mechanical Engineers: Seattle, WA, 2008; pp 655−662.

(5) Zhang, X.; Hu, D. Performance simulation of the absorption chiller using water and ionic liquid 1-ethyl-3-methylimidazolium dimethylphosphate as the working pair. *Appl. Therm. Eng.* **2011**, *31* (16), 3316−3321.

(6) Martin, A.; Bermejo, M. D. Thermodynamic analysis of absorption refrigeration cycles using ionic liquid + supercritical CO_2 pairs. *J. Supercrit. Fluids* **2010**, *55* (2), 852−859.

(7) Kim, Y. J.; Kim, S.; Joshi, Y. K.; Fedorov, A. G.; Kohl, P. A. Thermodynamic analysis of an absorption refrigeration system with ionic-liquid/refrigerant mixture as a working fluid. *Energy* **2012**, *44* (1), 1005−1016.

(8) Kim, S.; Kim, Y. J.; Joshi, Y. K.; Fedorov, A. G.; Kohl, P. A. Absorption heat pump/refrigeration system utilizing ionic liquid and hydrofluorocarbon refrigerants. *J. Electron. Packag.* **2012**, *134* (3), 031009-1−031009-9.

(9) Shiflett, M. B.; Yokozeki, A. Solubility and diffusivity of hydrofluorocarbons in room-temperature ionic liquids. *AIChE J.* **2006**, *52* (3), 1205−1219.

(10) Nie, N.; Zheng, D.; Dong, L.; Li, Y. Thermodynamic Properties of the Water + 1-(2-Hydroxylethyl)-3-methylimidazolium Chloride System. *J. Chem. Eng. Data* **2012**, *57* (12), 3598−3603.

(11) Yokozeki, A. Theoretical performances of various refrigerant−absorbent pairs in a vapor-absorption refrigeration cycle by the use of equations of state. *Appl. Energy* **2005**, *80* (4), 383−399.

(12) Welty, J. R. *Fundamentals of Momentum, Heat, and Mass Transfer*, 5th ed.; Wiley: Danvers, MA, 2008.

(13) Smith, J. M.; Van Ness, H. C.; Abbott, M. M. *Introduction to Chemical Engineering Thermodynamics*, 7th ed.; McGraw-Hill: Boston, MA, 2005.

(14) Yokozeki, A. Solubility of Refrigerants in Various Lubricants. *Int. J. Thermophys.* **2001**, *22* (4), 1057−1071.

(15) Yokozeki, A.; Shiflett, M. B. Water solubility in ionic liquids and application to absorption cycles. *Ind. Eng. Chem. Res.* **2010**, *49* (19), 9496−9503.

(16) Yokozeki, A.; Shiflett, M. B. Global phase behaviors of trifluoromethane in ionic liquid [bmim][PF_6]. *AIChE J.* **2006**, *52* (11), 3952−3957.

(17) Jacquemin, J.; Husson, P.; Padua, A. A. H.; Majer, V. Density and viscosity of several pure and water-saturated ionic liquids. *Green Chem.* **2006**, *8* (2), 172−180.

(18) Carey, V. P. *Liquid−Vapor Phase-Change Phenomena: An Introduction to the Thermophysics of Vaporization and Condensation Processes in Heat Transfer Equipment*; Hemisphere Publishing Corp.: Washington, DC, 1992.

(19) Lockhart, R. W.; Martinelli, R. C. Proposed correlation of data for isothermal two-phase, two-component flow in pipes. *Chem. Eng. Prog.* **1949**, *45* (1), 39−45.

(20) Lee, J.; Mudawar, I. Two-phase flow in high-heat-flux micro-channel heat sink for refrigeration cooling applications: Part I - Pressure drop characteristics. *Int. J. Heat Mass Transfer* **2005**, *48* (5), 928−940.

(21) Shah, R.; London, A. L. *Advances in Heat Transfer: Supplement*; Academic Press: New York, 1978; Vol. *1*.

(22) Zivi, S. Estimation of steady-state steam void-fraction by means of the principle of minimum entropy production. *J. Heat Transfer* **1964**, *86*, 247.

(23) Aphornratana, S.; Sriveerakul, T. Experimental studies of a single-effect absorption refrigerator using aqueous lithium−bromide: Effect of operating condition to system performance. *Exp. Therm. Fluid. Sci.* **2007**, *32* (2), 658−669.

NOTE ADDED AFTER ASAP PUBLICATION

This paper was published on the Web on May 1, 2013. References 11−13 were reordered, and the corrected version was reposted on May 15, 2013.